Materials Science-Poland, 34(1), 2016, pp. 169-176
http://www.materialsscience.pwr.wroc.pl/
DOI: 10.1515/msp-2016-0023

DE GRUYTER OPEN

VO_2(B) conversion to VO_2(A) and VO_2(M) and their oxidation resistance and optical switching properties

YIFU ZHANG*

School of Chemistry, Dalian University of Technology, Dalian 116024, PR China

Vanadium dioxide VO_2 has been paid in recent years increasing attention because of its various applications, however, its oxidation resistance properties in air atmosphere have rarely been reported. Herein, VO_2(B) nanobelts were transformed into VO_2(A) and VO_2(M) nanobelts by hydrothermal route and calcination treatment, respectively. Then, we comparatively studied the oxidation resistance properties of VO_2(B), VO_2(A) and VO_2(M) nanobelts in air atmosphere by thermo-gravimetric analysis and differential thermal analysis (TGA/DTA). It was found that the nanobelts had good thermal stability and oxidation resistance below 341 °C, 408 °C and 465 °C in air, respectively, indicating that they were stable in air at room temperature. The fierce oxidation of the nanobelts occurred at 426, 507 and 645 °C, respectively. The results showed that the VO_2(M) nanobelts had the best thermal stability and oxidation resistance among the others. Furthermore, the phase transition temperatures and optical switching properties of VO_2(A) and VO_2(M) were studied by differential scanning calorimetry (DSC) and variable-temperature infrared spectra. It was found that the VO_2(A) and VO_2(M) nanobelts had outstanding thermochromic character and optical switching properties.

Keywords: *VO_2 polymorphs; thermal properties; oxidation resistance; phase transition; optical properties*

1. Introduction

Over the past decades, numerous efforts have been employed in vanadium oxides and their related compounds as functional materials because of their layered structures, unique chemical and physical properties, which make them highly desired in a wide range of promising potential applications such as catalysts, cathode materials for reversible lithium batteries, gas sensors, intelligent thermochromic windows, electrical and optical devices, laser shield and so on [1–14]. As is well known, vanadium has abundant oxidation states (0 to +5), which usually correspond to a variety of binary oxides with the general formula VO_{2+x} ($-0.5 \leqslant x \leqslant 0.5$) [15, 16], such as V_2O_5, VO_2, V_2O_3, V_3O_7, V_4O_9, V_6O_{13}, etc. In the family of vanadium oxides, vanadium dioxide (VO_2) is a representative binary compound with different polymorphs, including VO_2(M), VO_2(R), VO_2(B), VO_2(A), VO_2(C), VO_2(D), etc. Among the VO_2 polymorphs, VO_2(B), VO_2(M/R) and VO_2(A) have been paid much attention in the past decades, and their crystallography data [17–20] are listed in Table 1.

VO_2(B) has attracted a great interest as a promising cathode material for Li-ion batteries, not only due to its proper electrode potential, but also its tunnel structure, through which Li-ions can make intercalation and de-intercalation in a reversible Li-ion battery [13, 21, 22]. Besides, VO_2(B) is usually used as a precursor to be transformed to VO_2(M/R) [22]. VO_2(M) shows a fully reversible first-order metal-to-insulator transition (MIT) with the phase transition temperature (T_c) at about 68 °C, accompanied by a crystallographic transition between a low temperature monoclinic phase (M) and a high temperature tetragonal phase (R) [23–27]. On warming, due to this transition, drastic changes occur in both electrical and optical properties below and above T_c. For instance, the infrared transmission characteristics of VO_2(M)

*E-mail: yfzhang@dlut.edu.cn

Table 1. The crystallography data of some important types of VO_2 polymorph.

Phase	T_c [°C]*	Cs*	Sg*	a [Å]	b [Å]	c [Å]	β(°)	Ref.
VO_2(B)	—	Monoclinic	C2/m	12.03	3.693	6.420	106.6	[17]
VO_2(M)	68	Monoclinic	$P2_1/c$	5.743	4.157	5.375	122.6	[18]
VO_2(R)	68	Tetragonal	$P4_2/mnm$	4.530	4.530	2.869	—	[19]
$VO_2(A_L)$	162	Tetragonal	P4/ncc	8.440	8.440	7.666	—	[20]
$VO_2(A_H)$	162	Tetragonal	I4/m	8.476	8.476	3.824	—	[20]

*T_c: phase transition temperature; Cs: Crystal system; Sg: Space group.

dramatically change over the phase transition and the change in electrical resistivity is of the order of 10^5 [23, 28]. These characteristics make VO_2(M) to be considered as a candidate for applications in smart window coatings, optical switching devices, intelligent energy conserving windows, electrical devices, laser protection, etc. [5, 6, 29–32]. Recently, an increasing attention has been paid to tetragonal VO_2(A) (space group P42/ncm) [26, 33, 34], because it shows a metal-semiconductor transition with the phase transition temperature (T_c) at 162 °C, accompanied by a crystallographic transition between a low temperature phase (LTP, P4/ncc, 130 °C below 162 °C) and a high temperature phase (HTP, I4/m, 87 °C above 162 °C). In the past decades, the synthesis, characterization and properties of VO_2(B), VO_2(M) and VO_2(A) have been extensively studied, however, the oxidation resistance properties of VO_2(B), VO_2(A) and VO_2(M) in air atmosphere have rarely been reported.

In this contribution, we first synthesized VO_2(B), VO_2(A) and VO_2(M) nanobelts and then studied their thermal behavior in air atmosphere. It was found that the as-obtained VO_2(B), VO_2(A) and VO_2(M) nanobelts had good thermal stability and oxidation resistance in air below 341 °C, 408 °C and 465 °C, respectively, indicating that the VO_2(M) nanobelts had the best thermal stability and oxidation resistance. Furthermore, the phase transition temperatures and optical switching properties of VO_2(A) and VO_2(M) were studied, and it was found that the VO_2(A) and VO_2(M) had outstanding thermochromic characteristics and optical switching properties.

2. Experimental

2.1. Materials

Vanadium pentoxide (V_2O_5), hydrogen peroxide (H_2O_2, 30 wt.%) and ethanol (CH_3CH_2OH) with analytical grade were purchased from Sinopharm Chemical Reagent Co., Ltd., and used without any further purification.

2.2. Synthesis of VO_2 (B) nanobelts

The synthesis of VO_2(B) nanobelts was based on our previous reports [22, 35] and slightly modified. In a typical synthesis, 0.455 g of commercial V_2O_5 was dispersed in 31 mL of redistilled water with magnetic stirring. Then 2 mL of H_2O_2 and 2 mL of ethanol were successively added into the solution, which was still stirred for 1 h at room temperature to obtain a brown liquid ($[VO(O_2)_2]^-$ solution), as shown in equation 1:

$$V_2O_5 + 4H_2O_2 \rightarrow 2[VO(O_2)_2]^- + 3H_2O + 2H^+ \quad (1)$$

After the solution achieved good homogeneity, the mixture was transferred into a 50 mL Teflon-lined stainless steel autoclave, then sealed and maintained at 180 °C for 48 h. When the reaction was finished, the blue-black precipitates were filtered off, washed with distilled water and anhydrous alcohol several times to remove any possible residues, and dried in vacuum at 75 °C for future applications.

2.3. Synthesis of VO_2(A) nanobelts transformed from VO_2(B) nanobelts

In a typical synthetic route for transforming VO_2(B) to VO_2(A), 0.50 g of the VO_2(B) nanobelts was dispersed into 40 mL of deionized water with magnetic stirring. The mixed solution was transferred into a 60 mL stainless steel autoclave after the solution became suspension. The autoclave was sealed and maintained at 280 °C for 48 h and then cooled to room temperature naturally. The products were filtered off, washed with distilled water and absolute ethanol several times to remove any possible residues, and dried in vacuum at 75 °C.

2.4. Synthesis of VO_2(M) nanobelts transformed from VO_2(B) nanobelts

In a typical transformation from VO_2(B) to VO_2(M), about 0.40 g of the VO_2(B) nanobelts were heated in a tube furnace with 5 °C/min heating rate under a high purity Ar (99.999 %) atmosphere at 700 °C for 2 h, and cooled to room temperature in the Ar flow to prevent the oxidation of VO_2(M).

2.5. Characterization

X-ray powder diffraction (XRD) study was carried out on D8 X-ray diffractometer equipment with Cu $K\alpha$ radiation, $\lambda = 1.54060$ Å. The data were collected between 5° and 70° with a scan speed of 4°/min. The morphology and dimensions of the products were observed by the transmission electron microscopy (TEM, JEM-2100). The sample was dispersed in absolute ethanol and was ultrasonicated before TEM. Thermogravimetric analysis and differential thermal analysis (TGA/DTA) were performed on SETSYS-1750 (AETARAM Instruments). About 10 mg of the sample was heated in an Al_2O_3 crucible in air atmosphere from ambient temperature to 700 °C at a constant rise of temperature (10 °C/min). The phase transition temperature (T_c) of VO_2(A) and VO_2(M) was measured by differential scanning calorimetry (DSC, DSC822^e, METTLER TOLEDO) with 5 °C/min heating rate. Optical properties of VO_2(A) and VO_2(M) were tested by variable-temperature Fourier transform infrared spectroscopy (IR, NICOLET 5700) with an adapted heating controlled cell. Variable-temperature IR patterns of the solid samples were measured using KBr pellet technique from 4000 to 400 cm^{-1} with a resolution of 4 cm^{-1}. About 1 wt.% of the samples and 99 wt.% of KBr were mixed homogeneously, and then the mixture was pressed into a pellet.

3. Results and discussion

3.1. Characterization of VO_2(B), VO_2(A) and VO_2(M) nanobelts

Fig. 1 depicts the typical XRD patterns of the as-prepared VO_2(B). All the diffraction peaks from Fig. 1b can readily be indexed to the monoclinic crystalline phase (space group C2/m) of VO_2(B) in agreement with the literature values (JCPDS Card No. 65-7960) [17], whose plots are shown in Fig. 1a. No impurity phases, such as V_2O_5, V_3O_7, V_6O_{13}, VO_2(M), VO_2(A) and V_2O_3, were detected, indicating high purity of the as-obtained VO_2(B).

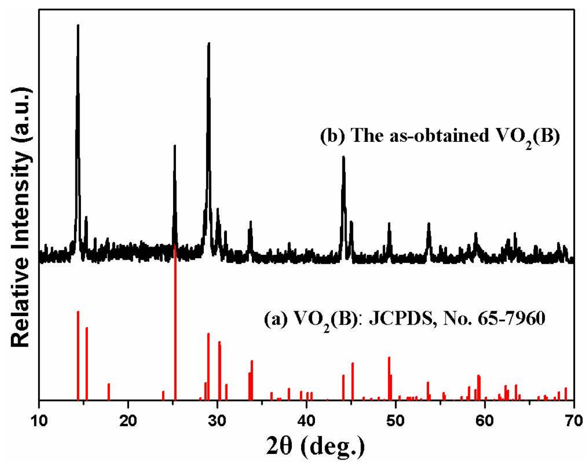

Fig. 1. XRD patterns of the as-obtained VO_2(B) nanobelts.

After hydrothermal treatment of VO_2(B) at 280 °C for 48 h, the XRD of the product has been measured and is shown in Fig. 2. It can be observed from Fig. 2 that all the diffraction peaks can readily be indexed to the tetragonal crystalline phase (space group: P42/ncm, No. 138) of VO_2(A) (JCPDS Card No. 42-0876) [36], indicating that the VO_2(A) was successfully transformed from VO_2(B). The as-prepared VO_2(A) is of high purity what can be inferred by comparing Fig. 2a and Fig. 2b. After calcination, VO_2(B) was transformed into VO_2(M), as shown in Fig. 3. All the diffraction peaks in Fig. 3b can readily be indexed to the monoclinic crystalline phase (space group: P21/c, No. 14) of VO_2(M) (JCPDS Card No. 72-0514) [18] and the as-prepared VO_2(M) is of high purity what can be stated by comparing Fig. 3a and Fig. 3b. Therefore, it can be said that VO_2(B), VO_2(A) and VO_2(M) were successfully prepared.

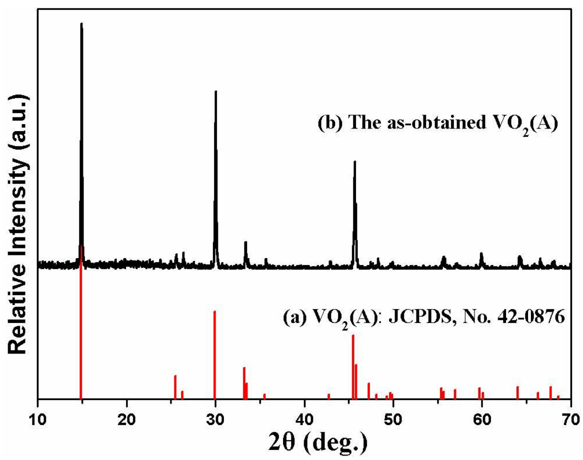

Fig. 2. XRD patterns of the as-obtained VO_2(A) transformed from VO_2(B) nanobelts by hydrothermal treatment at 280 °C for 48 h.

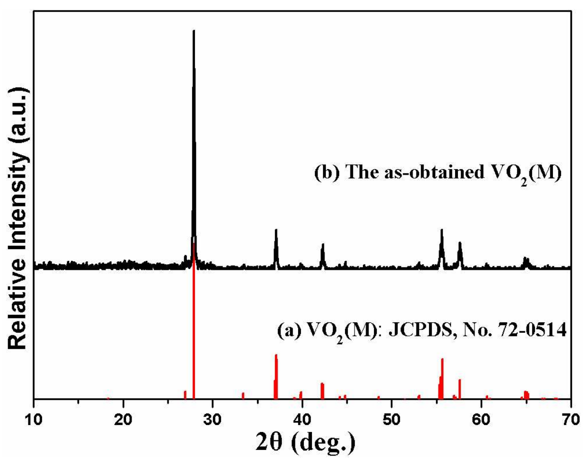

Fig. 3. XRD patterns of the as-obtained VO_2(M) transformed from VO_2(B) nanobelts by heating treatment at 700 °C for 2 h.

Fig. 4 shows the typical TEM images of the as-prepared VO_2(B), VO_2(A) and VO_2(M) nanobelts, which reveal that the as-obtained VO_2(B), VO_2(A) and VO_2(M) have similar morphology. The TEM images indicate that all of the as-obtained VO_2(B), VO_2(A) and VO_2(M) consist of a large number of 1D nanobelts with the length in the range of several to tens of micrometers and width ranging from 80 to 200 nm.

3.2. The oxidation resistance properties

In the past decades, VO_2(B), VO_2(A) and VO_2(M) nanobelts have been extensively studied, however, their oxidation resistance properties have not been reported in the literature. Therefore, in this contribution, the oxidation resistance properties of VO_2(B), VO_2(A) and VO_2(M) nanobelts were investigated by TGA/DTA with the flowing air, as shown in Fig. 5 and Fig. 6. Fig. 5 shows the TG curves of the as-obtained VO_2(B), VO_2(A) and VO_2(M) nanobelts in air atmosphere, which reveal that their oxidation process by O_2 starts at 341, 408 and 465 °C, respectively. The oxidation process of VO_2(B), VO_2(A) and VO_2(M) is finished at 472, 594 and 675 °C, respectively. The above results suggest that the VO_2(M) nanobelts have the best thermal stability and oxidation resistance. After the TGA/DTA test, a yellow powder was obtained, whose color is the same as that of V_2O_5, indicating that VO_2 is oxidized to V_2O_5.

As shown in Fig. 5, before beginning of VO_2 oxidation, the weight loss was not zero, which was caused by the loss of water absorbed on its surface. The weight loss of VO_2(B) is the largest while that of VO_2(M) is the least. The reason could be that VO_2(B) was directly prepared by a hydrothermal route and VO_2(M) was obtained by heating VO_2(B) at 700 °C, which could reduce the absorbed water. The weight loss of VO_2(B), VO_2(A) and VO_2(M) nanobelts in their oxidative process is 8.29, 9.01 and 9.54 %, respectively. The weight loss values of VO_2(B), VO_2(A) and VO_2(M) nanobelts correspond to the oxidation of the bulk VO_2 to V_2O_5 (9.64 %).

Fig. 6 shows the heat flow curves of the as-obtained VO_2(B), VO_2(A) and VO_2(M) nanobelts in air atmosphere, which suggests that the fierce oxidation of VO_2(B), VO_2(A) and VO_2(M) nanobelts

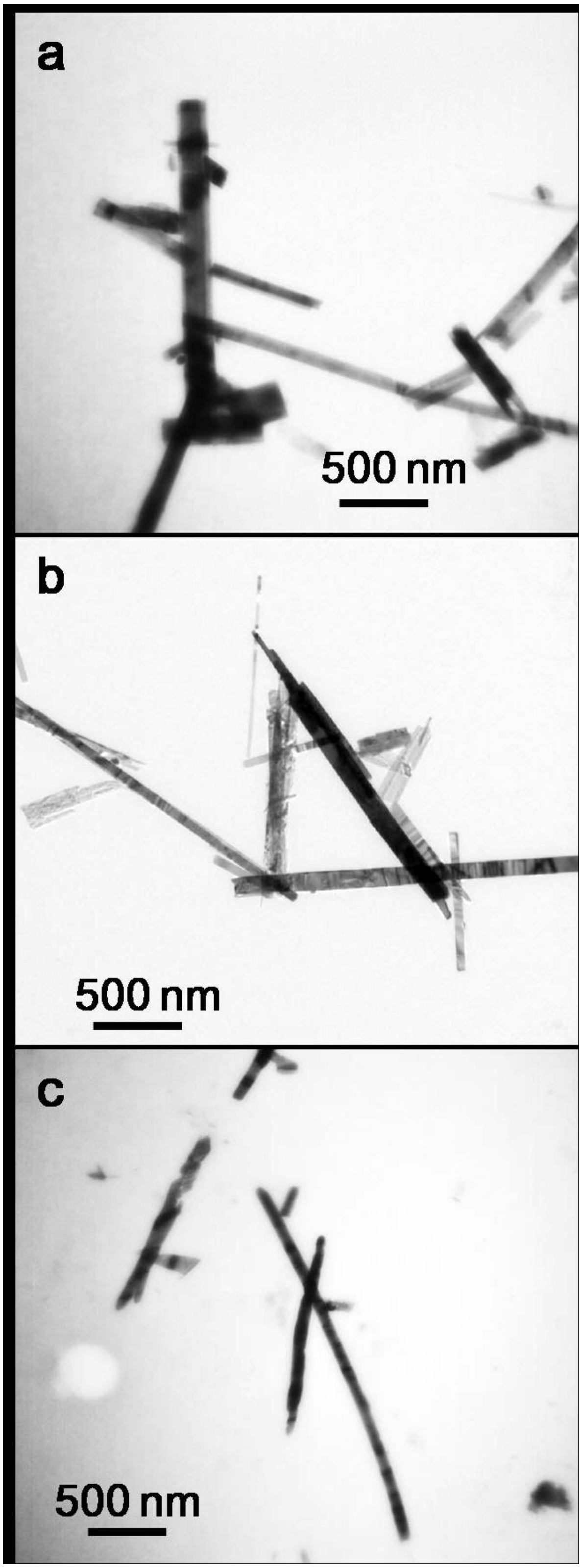

Fig. 4. TEM images of the as-obtained nanobelts: (a) VO_2(B), (b) VO_2(A) and (c) VO_2(M).

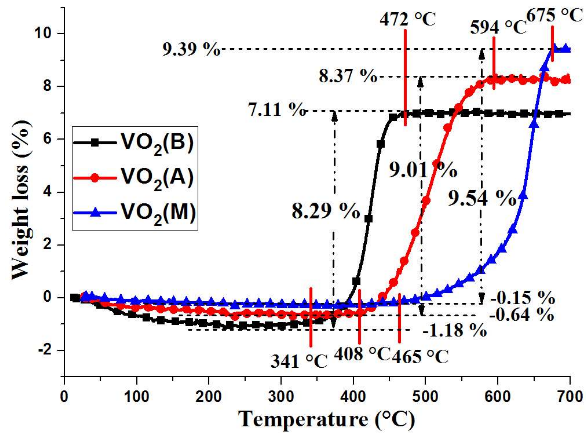

Fig. 5. TG curves of the as-obtained VO_2(B), VO_2(A) and VO_2(M) nanobelts in air atmosphere.

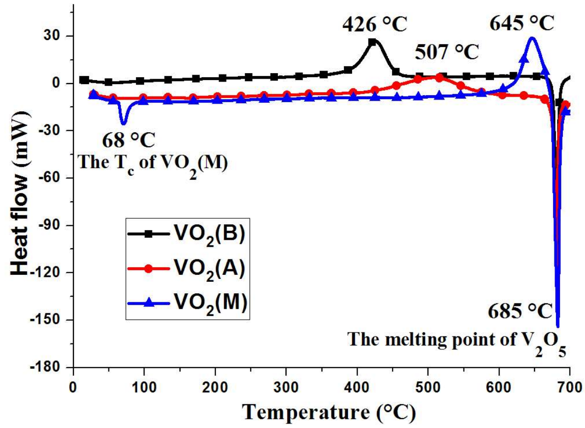

Fig. 6. Heat flow curves of the as-obtained VO_2(B), VO_2(A) and VO_2(M) nanobelts in air atmosphere.

occurs at 426, 507 and 645 °C, respectively. The sharp endothermic peak at about 685 °C is the melting point of V_2O_5, which further confirms that the oxidative product is V_2O_5. By the way, for VO_2(M) curve, a peak at 68 °C appears, which is the T_c of VO_2(M). Based on these results, it can be stated that the VO_2(B), VO_2(A) and VO_2(M) nanobelts have good thermal stability and oxidation resistance properties below 341, 408 and 465 °C in air atmosphere, respectively while the VO_2(M) nanobelts have the best thermal stability and oxidation resistance, which is beneficial for the application of VO_2(M) in air.

3.3. The phase transition and optical switching properties of VO_2(A) and VO_2(M) nanobelts

When the phase transition of VO_2(A) or VO_2(M) occurs, they exhibit a noticeable endothermal profile in the heating DSC curve, which corresponds to the phase transition of VO_2(A) or VO_2(M). Fig. 7 shows the typical DSC curves of VO_2(A) and VO_2(M). The T_c of VO_2(A) is about 162 °C, while for VO_2(M), the T_c is about 67 °C.

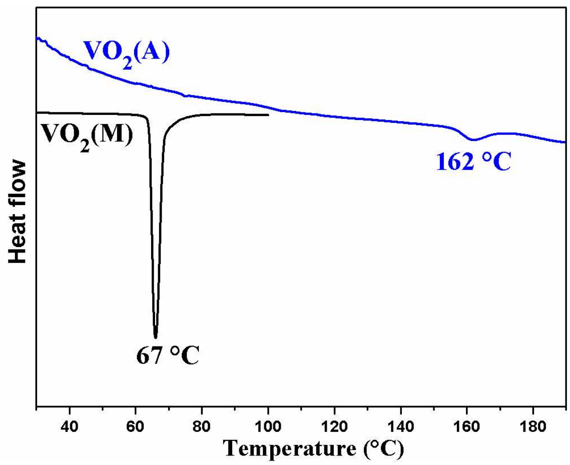

Fig. 7. DSC curves of the as-obtained VO_2(A) and VO_2(M) nanobelts.

According to the DSC results of the as-obtained VO_2(A) and VO_2(M), they reveal a noticeable endothermic peak in the heating cycle. It was reported that the optical properties have drastically changed when the reversible phase transition of VO_2(A) or VO_2(M) occurred. Therefore, we further developed the as-obtained VO_2(A) and VO_2(M) as the optical switching devices. The optical switching properties of VO_2(A) and VO_2(M) were investigated by variable-temperature infrared spectra, as shown in Fig. 8 and Fig. 9. It can be clearly seen from Fig. 8 that VO_2(A) has the optical switching properties at different vibratory absorption bands, revealing that it is a potential candidate for optical switching devices at the vibratory absorption bands from 700 to 650 cm^{-1} and from 600 to 550 cm^{-1}. In case of VO_2(M), as shown in Fig. 9, it can be clearly observed that VO_2(M) has the optical switching properties. The optical transmission below T_c is higher than that above T_c, suggesting that it has good thermochromic properties. Besides, it also reveals that VO_2(M) has potential applications in optical switching devices at the variety of vibratory absorption bands owing to its large transmission changes. These optical properties of VO_2(A) and VO_2(M) verify that they are beneficial for the development and application of optical switching materials.

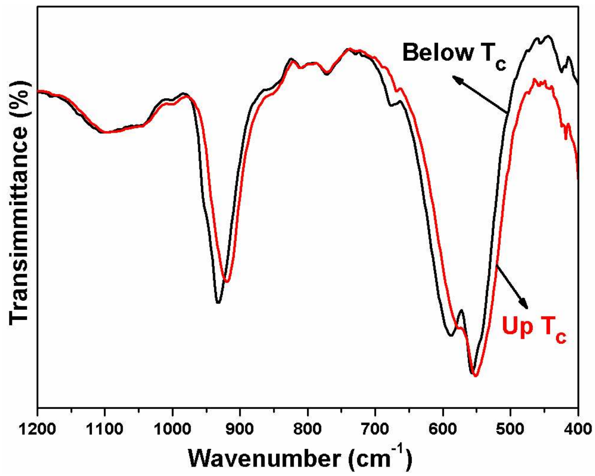

Fig. 8. Variable-temperature infrared spectra of VO_2(A) nanobelts below and above T_c.

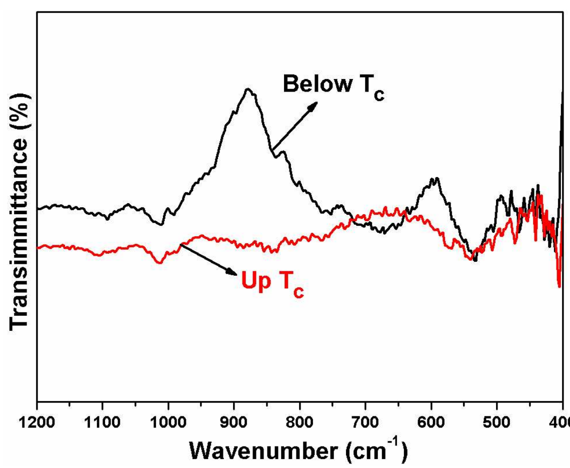

Fig. 9. Variable-temperature infrared spectra of VO_2(M) nanobelts below and above T_c.

It has been reported [1, 25, 34, 37–40] that the optical spectra, usually explained as the observed bands, are related to the electromagnetic resonance between incident photons (with a specific wavenumber) and variation of chemical bond polarization associated with a specific vibration mode. At low temperature ($T < T_c$) the electrons involved in the V^{4+}–V^{4+} bonds between VO_6 octahedra are localized. However, these electrons are delocalized at high temperature ($T > T_c$). In the metal state ($T > T_c$), this delocalization involves a screening effect for the incident photons, which occurs at the surface of the sample [37]. As a result, no vibrational absorption bands can be observed. In this circumstance, the transmittance drastically decreases. The variable-temperature infrared spectra confirm the strong reversible metal-insulator phase transition at around T_c.

4. Conclusions

In conclusion, the oxidation resistance properties of VO_2(B), VO_2(A) and VO_2(M) nanobelts were comparatively studied by TGA/DTA test. It was found that VO_2(B), VO_2(A) and VO_2(M) nanobelts had good thermal stability and oxidation resistance below 341 °C, 408 °C and 465 °C in air, respectively, and the fierce oxidation of the VO_2(B), VO_2(A) and VO_2(M) nanobelts occurred at 426, 507 and 645 °C, respectively. The results showed that VO_2(B), VO_2(A) and VO_2(M) nanobelts were stable in air at room temperature. VO_2(M) nanobelts had the best thermal stability and oxidation resistance, which was beneficial for the application of VO_2(M) in air. The T_c of VO_2(A) and VO_2(M) were about 162 °C and 67 °C, respectively. The optical switching properties of VO_2(A) and VO_2(M) were studied by the variable-temperature infrared spectra, which suggested that they can be used as the optical switching materials.

Acknowledgements

This work was partially supported by the Fundamental Research Funds for the Central Universities (DUT13RC(3)62) and the Science Research Project of the Liaoning Province Education Department (L2015123).

References

[1] ZHANG Y., ZHANG J., ZHANG X., MO S., WU W., NIU F., ZHONG Y., LIU X., HUANG C., LIU X., *J. Alloys Compd.*, 570 (2013), 104.

[2] ZHANG Y., WANG N., HUANG Y., HUANG C., MEI X., MENG C., *Mater Sci.-Poland*, 32 (2014), 236.

[3] STRELCOV E., LILACH Y., KOLMAKOV A., *Nano Lett.*, 9 (2009), 2322.

[4] ZHANG Y., FAN M., LIU X., HUANG C., LI H., *Eur. J. Inorg. Chem.*, 2012 (2012), 1650.

[5] ZHANG Y., FAN M., WU W., HU L., ZHANG J., MAO Y., HUANG C., LIU X., *Mater. Lett.*, 71 (2012), 127.

[6] PARKIN I.P., MANNING T.D., *J. Chem. Educ.*, 83 (2006), 393.

[7] ZHANG Y., LIU X., CHEN D., YU L., NIE J., YI S., LI H., HUANG C., *J. Alloy. Compd.*, 509 (2011), L69.

[8] ZHANG Y., ZHOU M., FAN M., HUANG C., CHEN C., CAO Y., LI H., LIU X., *Curr. Appl. Phys.*, 11 (2011), 1159.

[9] ZHANG Y., HUANG C., MENG C., *Mater. Express,* 5 (2015), 105.

[10] ZHANG Y., WANG N., HUANG Y., WU W., HUANG C., MENG C., *Ceram. Inter.*, 40 (2014), 11393.

[11] WANG N., ZHANG Y., HU T., ZHAO Y., MENG C., *Curr. Appl. Phys.*, 15 (2015), 493.

[12] KUMAR S., PICKETT M.D., STRACHAN J.P., GIBSON G., NISHI Y., WILLIAMS R.S., *Adv. Mater.*, 25 (42) (2013), 6128.

[13] WU C.Z., XIE Y., *Energ. Environ. Sci.*, 3 (2010), 1191.

[14] ZHANG Y., ZHANG X., HUANG Y., XIAO M., NIU F., HUANG C., MENG C., WU W., *Chem. Lett.*, 43 (3) (2014), 337.

[15] ZHANG Y., LIU X., XIE G., YU L., YI S., HU M., HUANG C., *Mater. Sci. Eng. B*, 175 (2010), 164.

[16] NGUYEN T.-D., DO T.-O., *Langmuir*, 25 (2009), 5322.

[17] THEOBALD F., CABALA R., BERNARD J., *J. Solid State Chem.*, 17 (1976), 431.

[18] ANDERSSON G., *Acta Chem. Scand.*, 10 (1956), 623.

[19] WESTMAN S., *Acta Chem. Scand.*, 15 (1961), 217.

[20] OKA Y., SATO S., YAO T., YAMAMOTO N., *J. Solid State Chem.*, 141 (1998), 594.

[21] NI J.A., JIANG W.T., YU K., GAO Y.F., ZHU Z.Q., *Electrochim. Acta*, 56 (2011), 2122.

[22] ZHANG Y., CHEN C., WU W., NIU F., LIU X., ZHONG Y., CAO Y., LIU X., HUANG C., *Ceram. Int.*, 39 (2013), 129.

[23] MORIN F.J., *Phys. Rev. Lett.*, 3 (1959), 34.

[24] GOODENOUGH J.B., *J. Solid State Chem.*, 3 (1971), 490.

[25] ZHANG Y., FAN M., NIU F., WU W., HUANG C., LIU X., LI H., LIU X., *Curr. Appl. Phys.*, 12 (2012), 875.

[26] ZHANG Y., HUANG Y., ZHANG J., WU W., NIU F., ZHONG Y., LIU X., LIU X., HUANG C., *Mater. Res. Bull.*, 47 (2012), 1978.

[27] ZHANG Y., ZHANG X., HUANG Y., HUANG C., NIU F., MENG C., TAN X., *Solid State Commun.*, 180 (2014), 24.

[28] ZYLBERSZTEJN A., MOTT N.F., *Phys. Rev. B*, 11 (1975), 4383.

[29] WHITTAKER L., WU T.L., PATRIDGE C.J., SAMBANDAMURTHY G., BANERJEE S., *J. Mater. Chem.*, 21 (2011), 5580.

[30] ZHANG Y., ZHANG J., ZHANG X., HUANG C., ZHONG Y., DENG Y., *Mater. Lett.*, 92 (2013), 61.

[31] JI S.D., ZHANG F., JIN P., *Mater. Lett.*, 65 (2011), 708.

[32] SON J.H., WEI J., COBDEN D., CAO G.Z., XIA Y.N., *Chem. Mater.*, 22 (2010), 3043.

[33] ZHANG S., SHANG B., YANG J., YAN W., WEI S., XIE Y., *Phys. Chem. Chem. Phys.*, 13 (2011), 15873.

[34] ZHANG Y., FAN M., NIU F., ZHONG Y., HUANG C., LIU X., WANG B., LI H., *Micro Nano Lett.*, 6 (2011), 888.

[35] ZHANG Y., LI W., FAN M., ZHANG F., ZHANG J., LIU X., ZHANG H., HUANG C., LI H., *J. Alloy. Compd.*, 544 (2012), 30.

[36] OKA Y., YAO T., YAMAMOTO N., *J. Solid State Chem.*, 86 (1990), 116.

[37] GUINNETON F., SAUQUES L., VALMALETTE J.C., CROS F., GAVARRI J.R., *J. Phys. Chem. Solids*, 62 (2001), 1229.

[38] RICHARDSON M.A., COATH J.A., *Opt. Laser Technol.*, 30 (1998), 137.

[39] CONTINENZA A., MASSIDDA S., POSTERNAK M., *Phys. Rev. B*, 60 (1999), 15699.

[40] ZHANG Y., FAN M., LIU X., XIE G., LI H., HUANG C., *Solid State Commun.*, 152 (2012), 253.

Received 2015-10-01
Accepted 2015-12-12